Spectrum Sharing Radar: Coexistence via Xampling

DEBORAH COHEN , Student Member, IEEE
KUMAR VIJAY MISHRA
YONINA C. ELDAR , Fellow, IEEE
Andrew and Erna Viterbi Faculty of Electrical Engineering, Technion–Israel Institute of Technology, Haifa, Israel

We present a Xampling-based technology enabling interference-free operation of radar and communication systems over a common spectrum. Our system uses a recently developed cognitive radio (CRo) to sense the spectrum at low sampling and processing rates. The Xampling-based cognitive radar (CRr) then transmits and receives in the available disjoint narrow bands. Our main contribution is the unification and adaptation of two previous ideas—CRo and CRr—to address spectrum sharing. Hardware implementation shows robust performance at SNRs up to –5 dB.

I. INTRODUCTION

The unhindered operation of a radar that shares its spectrum with communication ("comm," hereafter) systems has captured a great deal of attention within the operational radar community in recent years [1]–[3]. The interest in such *spectrum sharing* radars is largely due to electromagnetic spectrum being a scarce resource and almost all services having a need for a greater access to it. With the allocation of available spectrum to newer comm technologies, the radio frequency (RF) interference in radar bands is on the rise. Spectrum sharing radars aim to use the information from coexisting wireless and navigation services to manage this interference.

Recent research in spectrum sharing radars has focused on *S*- and *C*-band, where the spectrum has seen increasing cohabitation by long term-evolution (LTE) cellular/wireless commercial comm systems. Many synergistic efforts by major agencies are underway for efficient radio spectrum utilization. The enhancing access to the radio spectrum project by the national science foundation [3] brings together many different users for a flexible access to the electromagnetic spectrum. A significant recent development is the announcement of the shared spectrum access for radar and comm (SSPARC) program [2], [4] by the defense advanced research projects agency. This program is focused on *S*-band military radars and views spectrum sharing as a cooperative arrangement where the radar and comm services actively exchange information and do not ignore each other. It defines spectral *coexistence* as equipping existing radar systems with spectrum sharing capabilities and *spectral co-design* as developing new systems that utilize opportunistic access to the spectrum [5].

A variety of system architectures have been proposed for spectrum sharing radars. Most put emphasis on optimizing the performance of either radar or comm while ignoring the performance of the other. The radar-centric architectures [6]–[8] usually assume fixed interference levels from comm and design the system for high probability of detection (P_d). Similarly, the comm-centric systems (e.g., "CommRad" [9]) attempt to improve performance metrics like the error vector magnitude and bit/symbol error rate for interference from radar [10]. With the introduction of the SSPARC program, joint radar–comm performance is being investigated [11]–[13], with extensions to multiple input multiple output (MIMO) radar–comm [14]. In nearly all cases, real-time exchange of information between radar and comm hardware has not yet been integrated into the system architectures. Exceptions to this are automotive solutions where the same waveform is used for both target detection and comm [15], [16]. In a similar vein, our proposed method, described below, incorporates handshaking of spectral information between the two systems.

Conventional receiver processing techniques to remove RF interference in radar employ notch filters at hostile frequencies. If only a few frequencies are contaminated, then this method does not introduce exceedingly large signal distortion in radars that use wide bandwidths (e.g., FOliage

PENetration (FOPEN) [17]). An early work by Gerlach [18] suggests the use of step-frequency polyphase codes for ultrawideband radar waveforms to obtain a *thinned spectrum* with nulls at interfering frequencies. Later design solutions use convex optimization of radar performance metrics for given spectral constraints (see [19] and references therein; [20], [21]). The objective functions in such (convex and nonconvex) optimization procedures vary, where previous studies have considered signal-to-noise ratio (SNR) [22], transmit energy in stopband [7], sidelobe levels [23], a weighted sum of suppressed band spectral energy and range sidelobes [24], [25], and information theoretic metrics [26], [27]. A recent line of research focuses on constrained quadratic program techniques to obtain a waveform that fulfills more complex spectral constraints that take into account disturbance from overlaid licensed emitters [22], [28]. The radar is assumed to be aware of the radio environment map (REM) and optimization provides a coded transmit waveform. In all the above-mentioned works, spectrum sharing is achieved by notching out the radar waveform's bandwidth causing a decrease in the range resolution.

Our spectrum sharing solution departs from this baseline. The approach we adopt follows the recently proposed Xampling ("compressed sampling") framework [29], [30], a system architecture designed for sampling and processing of analog inputs at rates far below Nyquist, whose underlying structure can be modeled as a union of subspaces (UoS). The input signal belongs to a single subspace, *a priori* unknown, out of multiple, possibly even infinitely many, candidate subspaces. Xampling consists of two main functions: low rate analog to digital conversion (ADC), in which the input is compressed in the analog domain prior to sampling with commercial devices, and low rate digital signal processing, in which the input subspace is detected prior to digital signal processing. The resulting sparse recovery is performed using compressed sensing (CS) [31] techniques adapted to the analog setting. This concept has been applied to both comm [32]–[35] and radar [36], [37], among other applications.

Time-varying linear systems, which introduce both time shifts (delays) and frequency shifts (Doppler shifts), such as those arising in surveillance point-target radar systems, fit nicely into the UoS model. Here, a sparse target scene is assumed, allowing to reduce the sampling rate without sacrificing delay and Doppler resolution. The Xampling-based system is composed of an ADC that filters the received signal to predetermined frequencies before taking pointwise samples. These compressed samples, or "Xamples," contain the information needed to recover the desired signal parameters. In [36] and [38], a multiple bandpass sampling approach was adopted that used four groups of consecutive coefficients.

Here, we capitalize on the simple observation that if only narrow spectral bands are sampled and processed by the receiver, then one can restrict the transmit signal to these. The concept of transmitting only a few subbands that the receiver processes is one way to formulate a *cognitive radar* (CRr) [37]. The delay-Doppler recovery is then per-

formed as presented in [36]. The range resolution obtained through this multiband signal spectrum fragmentation can be the same as that of a wideband traditional radar. Further, by concentrating all the available power in the transmitted narrow bands rather than over a wide bandwidth, the CRr increases SNR. In the CRr system, as detailed in [37], the support of subbands varies with time to allow for dynamic and flexible adaptation to the environment. Such a system also enables the radar to disguise the transmitted signal as an electronic counter measure or cope with crowded spectrum by using a smaller interference-free portion. In this paper, we focus on this latter feature.

The CRr configuration is key to spectrum sharing since the radar transceiver adapts its transmission to available bands, achieving coexistence with comm signals. To detect such vacant bands, a comm receiver is needed that performs spectrum sensing over a large bandwidth. Such a task has recently received tremendous interest in the comm community, which faces a bottleneck in terms of spectrum availability. To increase the efficiency of spectrum managing, dynamic opportunistic exploitation of temporarily vacant spectral bands by secondary users has been considered, under the name of cognitive radio (CRo) [39], [40]. In this paper, we use a CRo receiver to detect the occupied comm bands, so that our radar transmitter can exploit the spectral holes. One of the main challenges of spectrum sensing in the context of CRo is the sampling rate bottleneck. This issue arises since CRos typically deal with wideband signals with prohibitively high Nyquist rates. Sampling at this rate would require very sophisticated and expensive ADCs, leading to a torrent of samples. In this context, the Xampling framework provides an analog preprocessing and sub-Nyquist sampling front end, and subsequent low rate digital recovery processing that exploits sparsity of the sensed signal in the frequency domain [32], [41]–[44].

Here, we propose a waveform design and receiver processing solution for spectral coexistence (as in SSPARC) composed of a comm receiver and radar transceiver implementing the Xampling concepts. The CRo comm receiver senses the spectrum from sub-Nyquist samples and provides the radar with spectral occupancy information. Equipped with this spectral map as well as a known REM detailing typical interference with respect to frequency, the CRr transmitter chooses narrow frequency subbands that minimize interference for its transmission. The delay-Doppler recovery is performed at the CRr receiver on these subbands. The combined CRo–CRr system results in spectral coexistence via the Xampling (SpeCX) framework, which optimizes the radar's performance without interfering with existing comm transmissions.

The main contribution of this paper is combining two previously proposed concepts, CRo and CRr, to solve an existing practical problem, comm–radar spectrum sharing. Beyond simple combination, the CRo and CRr are adapted to the specific comm–radar setting. First, the CRo processing is modified to the spectrum sharing scenario of comm signal detection in the presence of radar transmissions with known support. In addition, we consider the radar transmit

band selection problem conditioned on the comm detected spectrum. The CRr detection criterion, previously presented in terms of CS measures, is expressed here with respect to a radar setting. Finally, we present a hardware prototype for SpeCX that can perform real-time recovery of CRo and CRr signals sharing a common spectrum. Our prototype demonstrates recovery and spectrum sharing capabilities of the CRr at SNRs as low as -5 dB.

This paper is organized as follows. Section II reviews spectrum sharing research. Section III formulates the spectrum sharing problem and presents the comm and radar signal models. Section IV introduces our CRo comm receiver that performs blind spectrum sensing. In Section V, we describe the CRr transmitted band selection and corresponding delay-Doppler recovery. Software and hardware simulations are presented in Section VI.

II. SPECTRUM SHARING ACROSS IEEE RADAR BANDS

Spectral interference to radars has drastically increased with mobile comm technology. In this section, we review some of the main spectrum sharing applications. In the VHF (30–300 MHz) and UHF (300–1000 MHz) bands, interference comes from broadcast and TV services. A common example is the FOPEN radar, where the receiver is conventionally designed to notch out the interfering TV/radio frequencies [45]. Recent introduction of the IEEE 802.11ah protocol at 900 MHz for the Internet of Things, and 802.11af in 54–790 MHz for CRo technology makes VHF/UHF bands too crowded for smooth radar operation [46]. Some recent studies focus on designing passive systems that receive signals emitted by the new IEEE 802.22 standard devices which exploit the unused channels in the VHF and UHF bands allocated to television on a noninterfering and opportunistic basis. The primary objective of such white space [47], [48], cognitive and symbiotic radars [49] is to provide surveillance of critical infrastructure parameters by using radar technology.

From L-band (1–2 GHz) onward, radars begin to suffer spectral intrusion from LTE. An example is the air route surveillance radar used by Federal Aviation Administration sharing frequencies with wireless interoperability microwave access (WiMAX) devices [50]. Military radio services such as the joint tactical information distribution system in the 969–1206 MHz band are also known to interfere with L-band radars [51]. However, a majority of LTE waveforms, e.g., 802.11b/g/n (2.4 GHz) wideband code division multiplexing access, WiMAX LTE, LTE global system for mobile comm (GSM), enhanced data rates for GSM evolution, coexist within the S-band (2–4 GHz). Therefore, most of the spectrum sharing studies are concerned about S-band radars. A recent work [52] explores spectral cohabitation of Wi-Fi networks and S-band surveillance radars. LTE spectrum sharing is also being investigated for S-band shipborne air traffic control radars [53].

Spectral coexistence systems for C-band (4–8 GHz) are gradually gaining traction due to the latest 5-GHz band allocation to 802.11a/ac very high throughput wireless LAN

technology. In particular, this is of significant concern to the terminal weather doppler radar network, which is colocated with U.S. airports [54]. In fact, a recent study [55] identifies spectral interference threats from licensed transmitters to many other existing weather radar networks at S-, C-, and X-band.

At present, spectral crowding for surveillance or weather radars at frequencies higher than X-band is not under major investigation. However, in these bands, the automotive radar community has been more active in incorporating spectral cohabitation with comm services. For example, the work in [15] describes the "RadCom" system that combines a traffic sensing K-band automotive radar with a comm link to other vehicles. At V-band, another interesting study by Kumari *et al.* [16] shows that the 802.11ad Wi-Fi (60 GHz) Golay complementary sequence waveforms can also be used for radar remote sensing. Recently, applications of spectrum sharing in intervehicular comm and radar have also been proposed at W-band [56], [57]. Furthermore, with current waveform proposals for the 5G networks, centimeter (Ka), and millimeter (V and W) wavebands are expected to become dense in the future, thus requiring innovation in shared access to the spectrum [58]–[60]. In Section II, we formulate the spectrum sharing problem, where comm and radar transmit over a common bandwidth.

III. PROBLEM FORMULATION

Denote the set of all frequencies of the available common spectrum by $\mathcal{F}$. The comm and radar systems occupy subsets $\mathcal{F}_C$ and $\mathcal{F}_R$ of $\mathcal{F}$, respectively, such that $\mathcal{F}_C \cap \mathcal{F}_R = \emptyset$. Our goal is to design the radar waveform and its support $\mathcal{F}_R$, conditional on the fact that the comm occupies frequencies $\mathcal{F}_C$. We further assume that $\mathcal{F}_C$ itself is unknown to the comm receiver, which has to first detect these frequencies. The REM is assumed known to the system as a measure of the typical spectral interference with respect to frequency. Once $\mathcal{F}_C$ is identified, the comm receiver provides a spectral map of occupied bands to the radar. Equipped with the detected spectral map and known REM, the radar waveform generator selects the available bands with least interference for its transmission and notifies the radar receiver of its selection. The latter processes only these spectral bands using Xampling-based delay-Doppler recovery. The radar conveys the frequencies $\mathcal{F}_R$ to the comm receiver as well, so that it can ignore the radar bands while sensing the spectrum. Using our recovery methods, the CRr can achieve target detection and delay-Doppler estimation performance similar to that of a radar transmitting over the entire band $\mathcal{F}$ despite using only a fraction of this bandwidth.

Our model is that of a "friendly" spectral coexistence where active cooperation between radar and comm is required, as also envisaged by the SSPARC program. This is different than the spectrum sharing techniques where two systems operate independently of each other and attempt to minimize interference in their respective spectra.
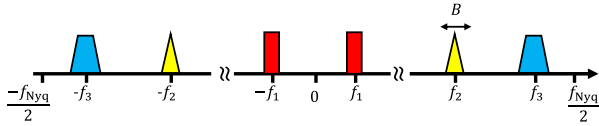
Fig. 1. Multiband model with $K = 6$ bands. Each band does not exceed the bandwidth B and is modulated by an unknown carrier frequency $|f_i| \leq f_{\text{Nyq}}/2$, for $i = 1, 2, 3$.

A. Multiband Comm Signal

Let $x_C(t)$ be a real-valued continuous-time comm signal, supported on $\mathcal{F} = [-1/2T_{\text{Nyq}}, +1/2T_{\text{Nyq}}]$ and composed of up to N_{sig} transmit waveforms such that

$$x_C(t) = \sum_{i=1}^{N_{\text{sig}}} s_i(t). \tag{1}$$

Formally, the Fourier transform of $x_C(t)$, defined by

$$X_C(f) = \lim_{T \to \infty} \frac{1}{\sqrt{T}} \int_{-T/2}^{T/2} x_C(t) e^{-j2\pi ft} dt \tag{2}$$

is zero for every $f \notin \mathcal{F}$. We denote by $f_{\text{Nyq}} = 1/T_{\text{Nyq}}$ the Nyquist rate of $x(t)$. The waveforms, respective carrier frequencies and bandwidths are unknown. We only assume that the single-sided bandwidth B_c^i for the ith transmission does not exceed an upper limit B, namely $B_c^i \leq B$ for all $1 \leq i \leq N_{\text{sig}}$. Such sparse wideband signals belong to the so-called *multiband signal model* [32], [61]. Fig. 1 illustrates the two-sided spectrum of a multiband signal with $K = 2N_{\text{sig}}$ bands centered around unknown carrier frequencies $|f_i| \leq f_{\text{Nyq}}/2$.

Let $\mathcal{F}_C \subset \mathcal{F}$ be the unknown support of $x_C(t)$, where

$$\mathcal{F}_C = \{f | |f - f_i| < B_c^i/2, \text{ for all } 1 \leq i \leq N_{\text{sig}}\}. \tag{3}$$

The goal of the comm receiver is to retrieve $\mathcal{F}_C$ while sampling and processing $x_C(t)$ at low rates in order to reduce system cost and resources.

B. Pulse Doppler Radar

Consider a standard pulse-Doppler radar that transmits a pulse train

$$r_{T_X}(t) = \sum_{p=0}^{P-1} h(t - p\tau), \quad 0 \leq t \leq P\tau \tag{4}$$

consisting of P uniformly spaced known pulses $h(t)$. The interpulse transmit delay τ is the pulse repetition interval (PRI) (or "fast time"); its reciprocal being the pulse repetition frequency (PRF). The entire duration of P pulses in (4) is known as the coherent processing interval, pulse dimension being the "slow time."

Assume that the radar target scene consists of L non-fluctuating point targets, according to the Swerling-0 target model [62]. The transmit signal is reflected back by the L targets and these echoes are received by the radar processor. The latter aims at recovering the following information about any of the L targets from the received signal: the time delay τ_l, which is linearly proportional to the range of the target from the radar; Doppler frequency ν_l, proportional to the radial velocity of the target with respect to the radar; and complex amplitude α_l, proportional to the target radar cross section, atmospheric attenuation, and other propagation factors. The target locations are defined with respect to the polar coordinate system of the radar and their range and Doppler are assumed to lie in the unambiguous time–frequency region, i.e., the time delays are no longer than the PRI and Doppler frequencies are up to the PRF. The received signal can then be written as

$$r_{R_X}(t) = \sum_{p=0}^{P-1} \sum_{l=0}^{L-1} \alpha_l h(t - \tau_l - p\tau) e^{-j\nu_l p\tau} + w(t) \tag{5}$$

for $0 \leq t \leq P\tau$, where $w(t)$ is a zero mean wide-sense stationary random signal with autocorrelation $r_w(s) = \sigma^2 \delta(s)$. It will be convenient to express $r_{R_X}(t)$ as a sum of single frames

$$r_{R_X}(t) = \sum_{p=0}^{P-1} r_{R_X}^p(t) + w(t) \tag{6}$$

where

$$r_{R_X}^p(t) = \sum_{l=0}^{L-1} \alpha_l h(t - \tau_l - p\tau) e^{-j\nu_l p\tau} \tag{7}$$

for $p\tau \leq t \leq (p+1)\tau$ is the return signal from the pth pulse.

In a conventional pulse Doppler radar, the pulse $h(t) = h_{\text{Nyq}}(t)$ is a time-limited baseband function whose continuous-time Fourier transform is $H_{\text{Nyq}}(f) = \int_{-\infty}^{\infty} h_{\text{Nyq}}(t) e^{-j2\pi ft} dt$. It is assumed that most of the signal's energy lies within the frequencies $\pm B_h/2$, where B_h denotes the effective signal bandwidth, such that the following approximation holds:

$$H_{\text{Nyq}}(f) \approx \int_{-B_h/2}^{B_h/2} h_{\text{Nyq}}(t) e^{-j2\pi ft} dt. \tag{8}$$

A classical radar signal processor samples each incoming frame $r_{R_X}^p(t)$ at the Nyquist rate B_h to yield the digitized samples $r_{R_X}^p[n]$, $0 \leq n \leq N - 1$, where $N = \tau B_h$. The signal enhancement process employs a matched filter for the sampled frames $r_{R_X}^p[n]$. This is then followed by Doppler processing where a P-point discrete Fourier transform (DFT) is performed on slow time samples. By stacking all the N DFT vectors together, a delay-Doppler map is obtained for the target scene. Finally, the time delays τ_l and Doppler shifts ν_l of the targets are located on this map using, e.g., a constant false-alarm rate detector.

The bandwidth B_h of the transmitted pulses governs the range resolution of the radar. Large bandwidth is necessary to obtain high resolution, but such a spectral requirement is at odds with the coexisting comm. We, therefore, propose an alternative efficient spectral utilization method wherein the radar transmits several narrow frequency bands instead of a full-band radar signal. In particular, we propose exploiting only a fraction of the bandwidth B_h for both transmission and reception of the radar signal, without degrading its

range resolution. In our spectrum sharing solution, the radar transmits a pulse $h(t)$ supported over N_b disjoint frequency bands, with bandwidths $\{B_r^i\}_{i=1}^{N_b}$ centered around the respective frequencies $\{f_r^i\}_{i=1}^{N_b}$, such that $\sum_{i=1}^{N_b} B_r^i < B_h$. The number of bands N_b is known to the receiver and does not change during the operation of the radar.

The location and extent of the bands B_r^i and f_r^i are determined by the radar transmitter through an optimization procedure to identify the least contaminated bands (see Section V-A). The resulting transmitted radar signal is

$$H_R(f) = \begin{cases} \beta_i H_{\text{Nyq}}(f), & f \in \mathcal{F}_R^i, \text{ for } 1 \leq i \leq N_b \\ 0, & \text{otherwise} \end{cases} \quad (9)$$

where $\mathcal{F}_R^i = [f_r^i - B_r^i/2, f_r^i + B_r^i/2]$ is the set of frequencies in the ith band.

The parameters $\beta_i > 1$ are chosen such that the total transmit power P_T of the spectrum sharing radar remains the same as that of the conventional radar

$$\int_{-B_h/2}^{B_h/2} |H_{\text{Nyq}}(f)|^2 \, df = \sum_{i=1}^{N_b} \int_{\mathcal{F}_r^i} |H_R(f)|^2 \, df = P_T. \quad (10)$$

In particular, if we choose $\beta_i = \beta$ for all $1 \leq i \leq N_b$ [63], then

$$\beta = \sqrt{\frac{\int_{-B_h/2}^{B_h/2} |H_{\text{Nyq}}(f)|^2 df}{\int_{\mathcal{F}_R} |H_R(f)|^2 \, df}} \quad (11)$$

where

$$\mathcal{F}_R = \bigcup_{i=1}^{N_b} \mathcal{F}_R^i. \quad (12)$$

IV. COGNITIVE RADIO

We assume that the comm signal is given by (1). When the frequency support of $x_C(t)$ is known, sampling methods such as demodulation, undersampling ADCs, and interleaved ADCs [30], [33] may be used to reduce the sampling rate below Nyquist. When the frequency locations of the transmissions are unknown, a classic processor samples $x(t)$ at its Nyquist rate f_{Nyq}, which can be prohibitively high. To overcome the sampling rate bottleneck, several blind sub-Nyquist sampling and recovery schemes have been proposed that exploit the signal's structure and in particular its sparsity in the frequency domain [32], [41]–[44]. It has been shown [61] that the minimal sampling rate for perfect blind recovery in multiband settings is twice the Landau rate [64], or twice the occupied bandwidth, namely $f_{\min} = 2\,\text{KB} = 4 N_{\text{sig}} B$. This rate can be significantly lower than Nyquist, by orders of magnitude.

In this paper, we focus on one such technique—the modulated wideband converter (MWC)—that achieves the lower sampling rate bound. The main advantage of the MWC is that it overcomes practical issues presented by other methods, allowing its hardware implementation. We first describe the MWC sub-Nyquist sampling scheme and then turn to signal recovery from low rate samples. We
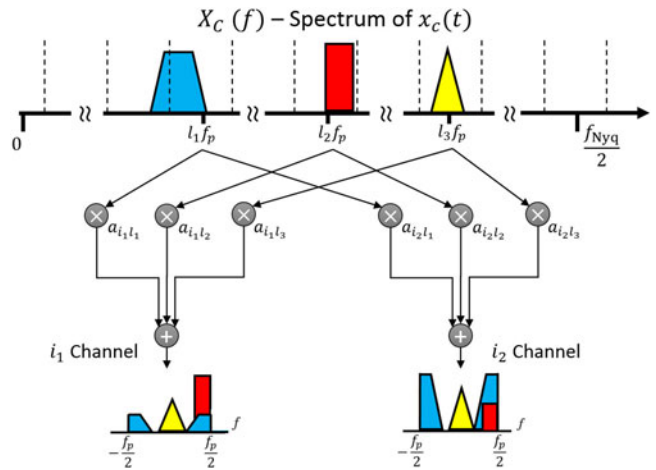

Fig. 2. Spectrum slices of the input signal $\mathbf{x}_C(f)$ multiplied by the coefficients a_{il} of the sensing matrix $\mathbf{A}$, resulting in the measurements $z_i(f)$ for the ith channel.

begin with a scenario where the radar is silent so that the signal sensed by the comm receiver is $x_C(t)$ and then extend our approach to include spectrum sensing in the presence of a known radar signal.

A. Sub-Nyquist Sampling

The MWC [32] is composed of M parallel channels. In each channel, an analog mixing front end, where $x_C(t)$ is multiplied by a mixing function $p_i(t)$, aliases the spectrum, such that each band appears in baseband. The mixing functions $p_i(t)$ are periodic with period T_p such that $f_p = 1/T_p \geq B$ and thus have the following Fourier expansion:

$$p_i(t) = \sum_{l=-\infty}^{\infty} c_{il} e^{j\frac{2\pi}{T_p} lt}. \quad (13)$$

In each channel, the signal goes through a low-pass filter (LPF) with cutoff frequency $f_s/2$ and is sampled at the rate $f_s \geq f_p$, resulting in the samples $z_i[n]$. Define

$$N = 2 \left\lceil \frac{f_{\text{Nyq}} + f_s}{2 f_p} \right\rceil \quad (14)$$

and $\mathcal{F}_s = [-f_s/2, f_s/2]$. Following the calculations in [32], the relation between the known discrete-time Fourier transform of the samples $z_i[n]$ and the unknown $X_C(f)$ is given by

$$\mathbf{z}(f) = \mathbf{A}\mathbf{x}_C(f), \qquad f \in \mathcal{F}_s \quad (15)$$

where $\mathbf{z}(f)$ is a vector of length N with ith element $z_i(f) = Z_i(e^{j2\pi f T_s})$ and the unknown vector $\mathbf{x}_C(f)$ is given by

$$\mathbf{x}_{Ci}(f) = X_C(f + (i - \lceil N/2 \rceil) f_p), \quad f \in \mathcal{F}_s \quad (16)$$

for $1 \leq i \leq N$. This relation is illustrated in Fig. 2. The $M \times N$ matrix $\mathbf{A}$ contains the known coefficients c_{il} such that

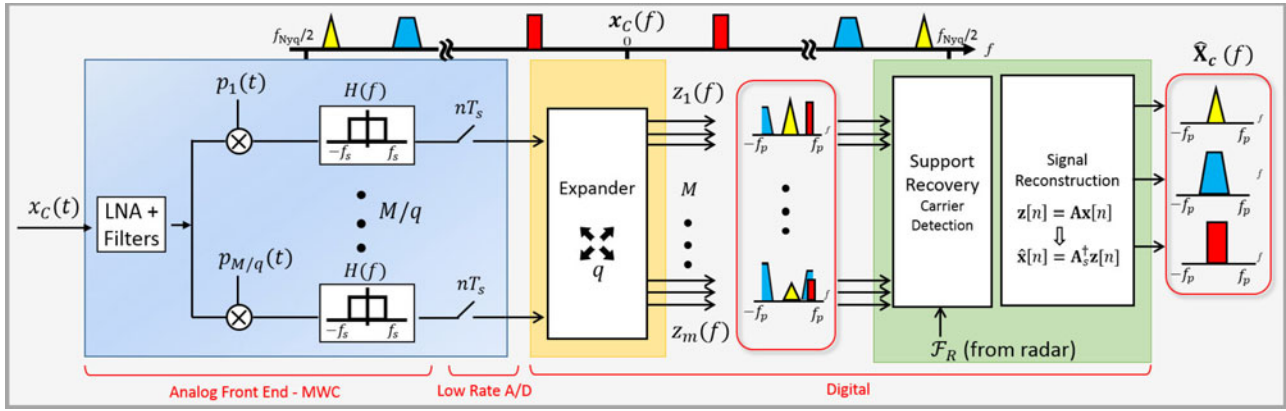$$\mathbf{A}_{il} = c_{i,-l} = c_{il}^*. \quad (17)$$

Fig. 3.   Schematic implementation of the MWC analog sampling front-end and digital signal recovery from low rate samples. The CRo inputs are the comm signal $x_C(t)$ and radar support $\mathcal{F}_R$. The comm support output $\mathcal{F}_C$ is shared with the radar transmitter.

The minimal number of channels to recover the K-sparse vector $\mathbf{x}_C(f)$, for $f \in \mathcal{F}_s$, dictated by CS results [31], is $M \geq 2K$ with $f_s \geq B$ per channel. The overall sampling rate, given by

$$f_{\text{tot}} = M f_s = \frac{M}{N} f_{\text{Nyq}} \qquad (18)$$

with $M < N$, can thus be as low as $f_{\min} = 2KB \ll f_{\text{Nyq}}$.

The number of branches M determines the total number of hardware devices and thus governs the level of hardware complexity. Reducing the number of channels is thus a crucial challenge for practical implementation of a CRo receiver. The MWC architecture presents an interesting flexibility property that permits trading channels for sampling rate, allowing to drastically reduce the number of channels. Consider a configuration where $f_s = q f_p$, with odd q. In this case, the ith physical channel provides q equations over $\mathcal{F}_p = [-f_p/2, f_p/2]$. Conceptually, M physical channels sampling at rate $f_s = q f_p$ are then equivalent to Mq channels sampling at $f_s = f_p$. The output of each of the M physical channels is digitally demodulated and filtered to produce samples that would result from Mq equivalent virtual branches. This happens in the so-called expander module, directly after the sampling stage. The number of channels is thus reduced at the expense of higher sampling rate f_s in each channel and additional digital processing. At its brink, this strategy allows to collapse a system with M channels to a single branch with sampling rate $f_s = M f_p$ (further details can be found in [30], [32], and [65]).

The MWC analog mixing front end, shown in Fig. 3, results in folding the spectrum to baseband with different weights for each frequency interval. The goal is now to recover $x_C(t)$, or alternatively $\mathbf{x}_C(f)$, from the low rate samples. In the next section, we provide a reconstruction algorithm that achieves the minimal rate of 2 KB.

B.   Signal Recovery

It is interesting to note that (15), which is written in the frequency domain, is valid in the time domain as well. We can therefore reconstruct $\mathbf{x}_C(f)$ in the frequency domain,

or alternatively, recover $\mathbf{x}_C[n]$ in the time domain using

$$\mathbf{z}[n] = \mathbf{A}\mathbf{x}_C[n]. \qquad (19)$$

The systems (15) and (19) are underdetermined due to the sub-Nyquist setup and known as infinite measurement vectors in the CS literature [30], [31]. With respect to these two properties, the digital reconstruction algorithm encompasses the following three stages [30], [61] that we explain in more detail below.

1) The continuous-to-finite (CTF) block constructs a finite frame (or basis) from the samples.
2) The support recovery formulates an optimization problem whose solution's support is identical to the support S_C of $\mathbf{x}_C[n]$, which is the active slices.
3) The signal can then be digitally recovered by reducing (19) to the support of $\mathbf{x}_C[n]$.

The recovery of $\mathbf{x}_C[n]$ for every n or $\mathbf{x}_C(f)$ for each f independently is inefficient and not robust to noise. Instead, the support recovery paradigm from [61] exploits the fact that the bands occupy continuous spectral intervals so that $\mathbf{x}_C(f)$ are jointly sparse for $f \in \mathcal{F}_p$, that is they have the same spectral support S_C. The CTF block [61] then produces a finite system of equations, called multiple measurement vectors (MMV) from the infinite number of linear systems (15) or (19).

From (15) or (19), we have

$$\mathbf{Q} = \Phi \mathbf{Z}_C \Phi^H \qquad (20)$$

where

$$\mathbf{Q} = \int_{f \in \mathcal{F}_p} \mathbf{z}(f)\mathbf{z}^H(f)df = \sum_{n=\infty}^{\infty} \mathbf{z}[n]\mathbf{z}^H[n] \qquad (21)$$

is a $M \times M$ matrix and

$$\mathbf{Z}_C = \int_{f \in \mathcal{F}_p} \mathbf{x}_C(f)\mathbf{x}_C^H(f)df = \sum_{n=-\infty}^{\infty} \mathbf{x}_C[n]\mathbf{x}_C^H[n] \qquad (22)$$

is a $N \times N$ matrix. The matrix $\mathbf{Q}$ is then decomposed to a frame $\mathbf{V}$ such that $\mathbf{Q} = \mathbf{V}\mathbf{V}^H$. Clearly, there are many possible ways to select $\mathbf{V}$. One possibility is to construct it

by performing an eigendecomposition of $\mathbf{Q}$ and choosing $\mathbf{V}$ as the matrix of eigenvectors corresponding to the nonzero eigenvalues. The finite dimensional MMV system

$$\mathbf{V} = \mathbf{A}\mathbf{U}_C \qquad (23)$$

is then solved for the sparsest matrix $\mathbf{U}_C$ with minimal number of nonidentically zero rows using CS techniques [30], [31]. The key observation of this strategy is that the support of the unique sparsest solution of (23) is the same as the support of our original set of equations (15) [61]. Recovering $\mathbf{U}_C$ from (23) can be performed using any MMV CS algorithm such as simultaneous orthogonal matching pursuit and simultaneous iterative hard thresholding [31].

Note that $\mathbf{x}_C(f)$ is K-sparse for each specific frequency $f \in \mathcal{F}_p$, whereas $\mathbf{x}_C[n]$ is $2K$-sparse since each transmission can split between two bins, as shown in Fig. 2 for the blue trapeze. After combining the frequencies, the matrix $\mathbf{U}_C$ is $2K$-sparse (at most) as well. Therefore, the above-mentioned algorithm referred to as SBR4 in [61] requires a minimal sampling rate of $2f_{\min}$. In order to achieve the minimal rate $f_{\min}$, the SBR2 algorithm regains the factor of two in the sampling rate at the expense of increased complexity [61]. In a nutshell, SBR2 is a recursive algorithm that alternates between the CTF described above and a bisection process. The bisection splits the original frequency interval into two equal width intervals on which the CTF is applied, until the level of sparsity of $\mathbf{U}_C$ is less or equal to K. As opposed to SBR4, which may be performed in both time and frequency, SBR2 can obviously be applied only in the frequency domain. We refer the reader to [61] for more details.

Once the support S_C is known, the slices of $x_C(t)$ are recovered either in the frequency or time domain by reducing the system of equations (15) or (19), respectively, to S_C. In the time domain, we have

$$\begin{aligned} \hat{\mathbf{x}}_C^{S_C}[n] &= \mathbf{A}_{S_C}^\dagger \mathbf{z}[n] \\ \hat{\mathbf{x}}_{C_i}[n] &= 0 \quad \forall i \notin S_C. \end{aligned} \qquad (24)$$

Here, $\hat{\mathbf{x}}_C^{S_C}[n]$ denotes the vector $\mathbf{x}_C[n]$ reduced to its support, $\mathbf{A}_{S_C}$ is composed of the columns of $\mathbf{A}$ indexed by S_C, and $\dagger$ is the Moore–Penrose pseudoinverse. The occupied comm support is then given by

$$\mathcal{F}_C = \{f \,||f - (i + \lceil N/2 \rceil)f_p| \leq \frac{f_p}{2}, \text{ for all } i \in S_C\}. \qquad (25)$$

A finer support can be estimated by performing energy detection on the recovered bands $\hat{\mathbf{x}}_C^{S_C}(f)$ for $f \in \mathcal{F}_p$. Last, if needed, the Nyquist rate samples $x[n] = x(nT_{\text{Nyq}})$ are reconstructed by summing the modulated and interpolated sequences $\mathbf{x}_C[n]$ to the Nyquist rate as

$$x[n] = \sum_{i \in S_c} (\hat{\mathbf{x}}_{C_i}[n] * h_I[n]) e^{j2\pi f_p n T_{\text{Nyq}}} \qquad (26)$$

where $h_I[n]$ is the digital interpolation filter. The MWC sampling and recovery processes are illustrated in Fig. 3.

C. Comm Signal Recovery in the Presence of Radar Transmission

In the previous section, we considered the scenario where the radar is silent and only the comm signal $x_C(t)$ is received. Here, we treat a more general setting in which the received signal is given by

$$x(t) = x_C(t) + x_R(t) \qquad (27)$$

where $x_R(t) = r_{T_x}(t) + r_{R_x}(t)$ is the radar signal sensed by the comm receiver, composed of the transmitted and received radar signals defined in (4) and (5), respectively. Following the derivations from the previous section, we can write the sub-Nyquist samples in the Fourier domain as

$$\mathbf{z}(f) = \mathbf{A}(\mathbf{x}_C(f) + \mathbf{x}_R(f)), \qquad f \in \mathcal{F}_s \qquad (28)$$

where

$$\mathbf{x}_{Ri}(f) = X_R(f + (i - \lceil N/2 \rceil)f_p), \quad 1 \leq i \leq N, f \in \mathcal{F}_s. \qquad (29)$$

The equation solved by the CTF then becomes

$$\mathbf{V} = \mathbf{A}(\mathbf{U}_C + \mathbf{U}_R). \qquad (30)$$

The frequency support $\mathcal{F}_R$ of $x_R(t)$, given by (12), is known at the comm receiver. From $\mathcal{F}_R$, we derive the support S_R of the radar slices $\mathbf{x}_R(f)$, which is identical to the support of $\mathbf{U}_R$, such that

$$S_R = \left\{ n \,\Big|\Big| n - \frac{f_R^i}{f_p} - \lceil N/2 \rceil \Big| < \frac{f_s + B_R^i}{2f_p} \right\} \qquad (31)$$

for $1 \leq i \leq N_b$. Our goal is then to recover the support of $\mathbf{U}_C$ from $\mathbf{V}$, given the known support S_R of $\mathbf{U}_R$. This can be formulated as sparse recovery with partial support knowledge, studied under the framework of modified CS [66], [67]. From [66], the minimal number of channels required for the exact reconstruction of the K-sparse matrix $\mathbf{U}_C$ is $M \geq 2K + |S_R|$.

The modified-CS framework has been used to adapt CS recovery algorithms to exploit partial known support (PKS). In particular, greedy algorithms, such as orthogonal matching pursuit (OMP) and iterative hard thresholding (IHT) have been modified to OMP with PKS (OMP-PKS) [68] and IHT-PKS [69], respectively. In OMP-PKS, instead of starting with an initial empty support set, one starts with S_R being the initial support set. The remainder of the algorithm is then identical to OMP. In each iteration of IHT-PKS, the estimator over the known support is kept and thresholding is performed only over the complementary support. Algorithm 1 summarizes the resulting sub-Nyquist comm signal recovery in the presence of radar transmission, using OMP-PKS for support recovery.

Performance improvement due to modified-CS is only achieved when the prior knowledge of the signal's partial support is fairly accurate. In case it is partially erroneous, one may consider the sparse Bayesian learning (SBL) framework that enables to automatically learn the true support from partially erroneous information. Algorithms such as MBP-DN [70], SA-SBL-SL [71], and CSA-

---

Algorithm 1: Cognitive Radio Spectrum Sensing.

Input: Observation vector $\mathbf{z}(f)$, $f \in \mathcal{F}_s$, radar support $\mathcal{F}_R$

Output: Comm signal support $\mathcal{F}_C$ and slices estimate $\hat{\mathbf{x}}_C[n]$

1: Compute the support S_R as in (31)
2: Compute $\mathbf{Q}$ from (21) and extract a frame $\mathbf{V}$ such that $\mathbf{Q} = \mathbf{V}\mathbf{V}^H$ using eigendecomposition
3: Compute the estimate

$$\hat{\mathbf{U}}_1^{S_R} = \mathbf{A}_{S_R}^\dagger \mathbf{V}, \quad \hat{\mathbf{U}}_{1_i} = \mathbf{0}, \quad \forall i \notin S_R$$

4: Compute the residual

$$\mathbf{V}_1 = \mathbf{V} - \mathbf{A}_{S_R}\hat{\mathbf{U}}_1$$

5: Find the total signal support $S_R \bigcup S_C$ using OMP from the second iteration with sampling matrix $\mathbf{A}$, residual $\mathbf{V}_1$ and support S_R
6: Find the comm (and radar) slices estimate from

$$\hat{\mathbf{x}}^{S_C \bigcup S_R}[n] = \mathbf{A}_{S_C \bigcup S_R}^\dagger \mathbf{z}[n],$$

$$\hat{\mathbf{x}}_i[n] = 0, \quad \forall i \notin S_C \bigcup S_R$$

7: Compute the comm signal support $\mathcal{F}_C$ from (25)

SBL [72] are able to correct the erroneous prior knowledge on the support $\mathcal{F}_C$ and learn the clustering pattern of the true signal.

V. COGNITIVE RADAR

Once the set $\mathcal{F}_C$ is estimated, the objective of the radar is to identify an appropriate transmit frequency set $\mathcal{F}_R \subset \mathcal{F} \setminus \mathcal{F}_C$ such that the radar's probability of detection P_d is maximized. For a fixed probability of false alarm P_{fa}, the P_d increases with higher signal-to-interference-and-noise ratio (SINR) [73]. Hence, the frequency selection process can, alternatively, choose to maximize the SINR or minimize the spectral power in the undesired parts of the spectrum. At the receiver of this spectrum sharing radar, we employ the sub-Nyquist approach described in [36], where the delay-Doppler map is recovered from the subset of Fourier coefficients defined by $\mathcal{F}_R$.

A. Optimal Radar Transmit Bands

The REM is assumed to be known to the radar transmitter in the form of typical interfering energy levels with respect to frequency bands, represented by a vector $\mathbf{y} \in \mathbb{R}^q$, where q is the number of frequency bands with bandwidth $b_y \triangleq |\mathcal{F}|/q$. The radar measures the REM vector $\mathbf{y}$ (in dBm) in passive mode by sweeping over $\mathcal{F}$. In addition, the information available from the CRo indicates that the radar waveform must avoid all the frequencies in the set $\mathcal{F}_C$. Therefore, we further set $\mathbf{y}$ to be equal to ∞ in the bands that coincide with $\mathcal{F}_C$. The goal is now to select subbands from the set $\mathcal{F} \setminus \mathcal{F}_C$ with minimal interference energy. We thus seek a block-sparse frequency vector $\mathbf{w} \in \mathbb{R}^p$ with unknown block lengths, where p is the number of discretized frequen-

cies, and whose support provides frequency bands with low interference for the radar transmission. Each entry of $\mathbf{w}$ represents a frequency subband of bandwidth $b_w \triangleq |\mathcal{F}|/p$.

To this end, we use the structured sparsity framework from [74] that extends standard sparsity regularization to structured sparsity. We adopt the one-dimensional graph sparsity structure to represent frequencies. The p nodes are the ordered entries of $\mathbf{w}$, so that neighbor nodes are indexed by adjacent frequency bands. Block sparsity is enforced by encouraging the graph to contain connected regions, which, in the context of our problem, correspond to low inference frequency subbands for radar transmission. In contrast to traditional block-sparsity approaches [31], this formulation does not require *a priori* knowledge on the location of the nonzero blocks. This is achieved by replacing the traditional sparse recovery ℓ_0 constraint by a more general term $c(\mathbf{w})$, referred to as the coding complexity, such that

$$c(\mathbf{w}) = \min_F \{c(F)|\text{supp}(\mathbf{w}) \subset F\} \qquad (32)$$

where $F \subset \{1, \ldots, p\}$ is a sparse subset of the index set of the coefficients of $\mathbf{w}$. That is, F is the set of chosen frequencies. In particular, for graph sparsity, the choice of $c(F)$ is simply

$$c(F) = g \log p + |F| \qquad (33)$$

where g is the number of connected regions, or blocks, of F, namely radar subbands. This coding complexity, which accounts for both the number of discretized frequencies $|F|$ and the number of connected regions g, favors blocks within the graph.

The resulting optimization problem for finding the block-sparse frequency vector $\mathbf{w}$ can then be expressed as

$$\min_{\mathbf{w}} \; ||\mathbf{y}_{\text{inv}} - \mathbf{D}\mathbf{w}||_2^2 + \lambda c(\mathbf{w}) \qquad (34)$$

where λ is a regularization parameter and $c(\mathbf{w})$ is defined in (32) with $c(F)$ in (33). Here, $\mathbf{y}_{\text{inv}}$ contains elementwise reciprocals of $\mathbf{y}$, namely $(\mathbf{y}_{\text{inv}})_i = 1/\mathbf{y}_i$, so that small values in $\mathbf{y}_{\text{inv}}$ induce corresponding zero blocks in $\mathbf{w}$, and $\mathbf{D}$ is a $q \times p$ matrix that maps each discrete frequency in $\mathbf{w}$ to the corresponding band in $\mathbf{y}_{\text{inv}}$. That is, the (i, j)th entry of $\mathbf{D}$ is equal to 1 if the jth frequency in $\mathbf{w}$ belongs to the ith band in $\mathbf{y}$; otherwise, it is equal to 0. If we choose $p = q$, then $\mathbf{D} = \mathbf{I}$ is the $q \times q$ identity matrix.

Problem (34) can be solved using a structured greedy algorithm, structured OMP (StructOMP), presented in [74] and adapted to our setting in Algorithm 2. In [74], the algorithm proceeds by greedily adding blocks one at a time to reduce the loss, scaled by the cost of the added block. Here, we consider single element blocks for simplicity but larger blocks can be considered to increase the algorithm's effectiveness. In the original StructOMP [74], the stopping criterion is based on additional *a priori* information on the overall sparsity and number of nonzero blocks. We adopt an alternative stopping criterion, based only on the number of blocks, which is known to be equal to N_b in our problem. This leads to N_b bands in $\mathcal{F}_R$ as dictated by the hardware constraints. Besides the requirement on the num-

Algorithm 2: Cognitive Radar Band Selection.

Input: REM vector **y** and subbands bandwidth
$b_y = |\mathcal{F}|/q$, shared support $\mathcal{F}$, comm support
$\mathcal{F}_C$, mapping matrix **D**, number of discretized
frequencies p, number of bands N_b

Output: Block-sparse vector **w**, radar support $\mathcal{F}_R$

1: Set $\mathbf{y}_i = \infty$, for all $1 \leq i \leq q$ such that $[ib_y - |\mathcal{F}|/2, (i+1)b_y - |\mathcal{F}|/2] \bigcap \mathcal{F}_C \neq \emptyset$ and compute $(\mathbf{y}_{\text{inv}})_i = 1/\mathbf{y}_i$

2: Initialization $F_0 = \emptyset$, $\mathbf{w} = \mathbf{0}$, $t = 1$

3: Find the index λ_t so that $\lambda_t = \arg\max \phi(i)$, where

$$\phi(i) = \frac{||\mathbf{P}_i(\mathbf{D}\hat{\mathbf{w}}_{t-1} - \mathbf{y}_{\text{inv}})||_2^2}{c(i \bigcup F_{t-1}) - c(F_{t-1})}$$

with $\mathbf{P}_i = \mathbf{D}_i(\mathbf{D}_i^T \mathbf{D}_i)^\dagger \mathbf{D}_i^T$

4: Augment index set $F_t = \lambda_t \bigcup F_{t-1}$

5: Find the new estimate

$$\hat{\mathbf{w}}_{t|F_t} = \mathbf{D}_{F_t}^\dagger \mathbf{y}_{\text{inv}}, \quad \hat{\mathbf{w}}_{t|F_t^C} = \mathbf{0}$$

6: If the number of blocks, or connected regions, $g(\mathbf{w}) > N_b$, go to step 7. Otherwise, return to step 3

7: Remove the last index λ_t so that $F_t = F_{t-1}$ and $\hat{\mathbf{w}}_t = \hat{\mathbf{w}}_{t-1}$

8: Compute the radar support

$$\mathcal{F}_R = \bigcup_{j \in F_t} [jb_w - |\mathcal{F}|/2, (j+1)b_w - |\mathcal{F}|/2]$$

with $b_w = |\mathcal{F}|/p$

---

ber of blocks to be N_b, the total bandwidth $|\mathcal{F}_R|$ should be large enough to fulfill (42), as explained in the next section. In case the N_b bands are reached and the total bandwidth is not satisfied, then the minimum size of the bands must be changed and a new search should be initiated.

In the above, additional requirements of transmit power constraints, range sidelobe levels, and minimum separation between the bands may also be imposed and, if needed, alternative block-SBL algorithms that require none (e.g., Cluss-MCMC [75], [76] and DGS [77]) or very little *a priori* knowledge (e.g., B-SBL [78], Cluster-SBL [79], and PC-SBL [80]) can be used. These methods yield more accurate solutions at the cost of execution time. Once the support $\mathcal{F}_R$ is identified, a suitable waveform code may be designed using optimization procedures described by, e.g., [22] and [25].

B. Delay-Doppler Recovery

We now turn to the radar receiver design and describe how a delay-Doppler map can be recovered from only N_b transmitted narrow bands. The radar receiver first filters the CRr subbands supported on $\mathcal{F}_R$ given by (12) and computes the Fourier coefficients of the received signal. The width of the subbands is determined by the search process described in the previous section. The maximum width is limited by the passband response of the receive filters.
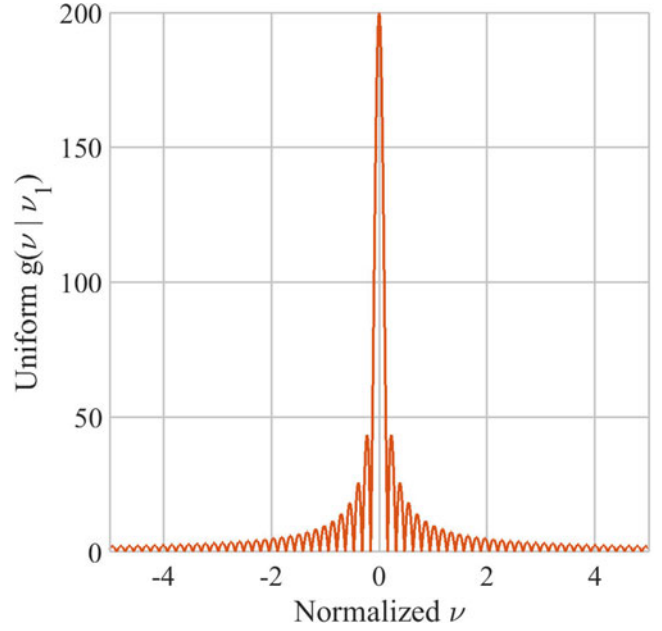

Fig. 4. Sum of exponents $|g(\nu|\nu_l)|$ for $P = 200$, $\tau = 1$ s and $\nu_l = 0$.

Consider the Fourier series representation of the aligned frames $r_{R_X}^p(t + p\tau)$, with $r_{R_X}^p(t)$ defined in (7)

$$c_p[k] = \int_0^\tau r_{R_X}^p(t + p\tau)e^{-j2\pi kt/\tau}dt$$
$$= \frac{1}{\tau}H[k]\sum_{l=0}^{L-1}\alpha_l e^{-j2\pi k\tau_l/\tau}e^{-j\nu_l p\tau} \quad (35)$$

for $k \in \kappa$, where $\kappa = \left\{k = \left\lfloor \frac{f}{f_{\text{Nyq}}}N \right\rfloor \,\bigg|\, f \in \mathcal{F}_R\right\}$. From (35), we see that the unknown parameters $\{\alpha_l, \tau_l, \nu_l\}_{l=0}^{L-1}$ are embodied in the Fourier coefficients $c_p[k]$. The goal is then to recover these parameters from $c_p[k]$ for $k \in \kappa$ and $0 \leq p \leq P - 1$.

To that end, we adopt the Doppler focusing approach from [36]. Consider the DFT of the coefficients $c_p[k]$ in the slow time domain

$$\tilde{\Psi}_\nu[k] = \sum_{p=0}^{P-1} c_p[k]e^{j\nu p\tau}$$
$$= \frac{1}{\tau}H[k]\sum_{l=0}^{L-1}\alpha_l e^{-j2\pi k\tau_l/\tau}\sum_{p=0}^{P-1}e^{j(\nu-\nu_l)p\tau}. \quad (36)$$

The key to Doppler focusing follows from the approximation

$$g(\nu|\nu_l) = \sum_{p=0}^{P-1}e^{j(\nu-\nu_l)p\tau} \approx \begin{cases} P & |\nu - \nu_l| < \pi/P\tau \\ 0 & |\nu - \nu_l| \geq \pi/P\tau \end{cases} \quad (37)$$

as illustrated in Fig. 4. Denote the normalized focused measurements $\Psi_\nu[k]$ so that

$$\Psi_\nu[k] = \frac{\tau}{PH[k]}\tilde{\Psi}_\nu[k]. \quad (38)$$

As in traditional pulse-Doppler radar, suppose we limit ourselves to the Nyquist grid so that $\tau_l/\tau = r_l/N$, where

Algorithm 3: Cognitive Radar.
___

Input: Observation vectors $c_p[k]$, for all $0 \le p \le p - 1$ and $k \in \kappa$, probability of false alarm P_{fa}, noise variance σ^2, transmitted power P_T, total transmitted bandwidth $|\mathcal{F}_R|$

Output: Estimated target parameters $\{\hat{\alpha}_l, \hat{\tau}_l, \hat{\nu}_l\}_{l=0}^{L-1}$

1: Create Ψ from $c_p[k]$ using the fast Fourier transform (FFT) (36), for $k \in \kappa$ and $\nu = -1/(2\tau)$ $+ p/(P\tau)$ for $0 \le p \le P - 1$

2: Compute detection thresholds

$$\rho = \frac{P_T}{\sigma^2 |\mathcal{F}_R|}, \quad \gamma = Q_{\chi_2^2(\rho)}^{-1}(1 - \sqrt[N]{1 - P_{\text{fa}}})$$

3: Initialization: residual $\mathbf{R}_0 = \Psi$, index set $\Lambda_0 = \emptyset$, $t = 1$

4: Project residual onto measurement matrix:

$$\Phi = \mathbf{F}_\kappa^H \mathbf{R}_{t-1}$$

5: Find the two indices $\lambda_t = [\lambda_t(1) \quad \lambda_t(2)]$ such that

$$[\lambda_t(1) \quad \lambda_t(2)] = \arg\max_{i,j} |\Phi_{i,j}|$$

6: Compute the test statistic

$$\Gamma = \frac{(\mathbf{F}_\kappa)_{\lambda_t(1)}((\mathbf{R}_{t-1})_{\lambda_t(2)})^H((\mathbf{F}_\kappa)_{\lambda_t(1)})^H(\mathbf{R}_{t-1})_{\lambda_t(2)}}{\sigma^2}$$

where $(\mathbf{M})_i$ denotes the ith column of $\mathbf{M}$

7: If $\Gamma > \gamma$ continue, otherwise go to step 12

8: Augment index set $\Lambda_t = \Lambda_t \bigcup \{\lambda_t\}$

9: Find the new signal estimate

$$\hat{\mathbf{X}}_{t|\Lambda_t} = (\mathbf{F}_\kappa)_{\Lambda_t}^\dagger \Psi, \quad \hat{\mathbf{X}}_{t|\Lambda_t^C} = \mathbf{0}$$

10: Compute new residual

$$\mathbf{R}_t = \Psi - (\mathbf{F}_\kappa)_{\Lambda_t} \hat{\mathbf{X}}$$

11: Increment t and return to step 4

12: Estimated support set $\hat{\Lambda} = \Lambda_t$

13: $\hat{\tau}_l = \frac{\tau}{N}\hat{\Lambda}(l, 1)$, $\hat{\nu}_l = \frac{1}{P\tau}\hat{\Lambda}(l, 2)$, $\hat{\alpha}_l = \hat{\mathbf{X}}_{\hat{\Lambda}(l,1),\hat{\Lambda}(l,2)}$
___

r_l is an integer satisfying $0 \le r_l \le N - 1$. Then, (38) can be approximately written in vector form as

$$\Psi_\nu = \mathbf{F}_\kappa \mathbf{x}_\nu \tag{39}$$

where $\Psi_\nu = [\Psi_\nu[k_0], \ldots, \Psi_\nu[k_{K-1}]]$, $k_i \in \kappa$ for $0 \le i \le K - 1$, $\mathbf{F}_\kappa$ is composed of the K rows of the $N \times N$ Fourier matrix indexed by κ, and $\mathbf{x}_\nu$ is a L-sparse vector that contains the values α_l at the indices r_l for the Doppler frequencies ν_l in the "focus zone," that is $|\nu - \nu_l| < \pi/P\tau$. It is convenient to write (39) in matrix form, by vertically concatenating the vectors Ψ_ν, for ν on the Nyquist grid, namely $\nu = -\frac{1}{2\tau} + \frac{1}{P\tau}$, into the $K \times P$ matrix Ψ, as

$$\Psi = \mathbf{F}_\kappa \mathbf{X}. \tag{40}$$

The P equations (39) can be solved simultaneously using Algorithm 3, where in each iteration, the maximal projection of the observation vectors onto the measurement matrix are retained. The algorithm termination criterion

follows from the generalized likelihood ratio test (GLRT) based framework presented in [81]. For each iteration, the alternative and null hypotheses in the GLRT problem define the presence or absence of a candidate target, respectively. In the Algorithm, $Q_{\chi_2^2}(\rho)$ denotes the right-tail probability of the chi-square distribution function with two degrees of freedom, Λ^C is the complementary set of Λ and

$$\rho = \frac{P_T}{\sigma^2 |\mathcal{F}_R|} \tag{41}$$

is the SNR with σ^2 the noise variance and P_T defined in (10).

The following theorem from [36] derives a necessary condition on the minimal number of samples K and pulses P for perfect recovery in a *noiseless* environment.

THEOREM 1 (SEE [36]): The minimal number of samples required for perfect recovery of $\{\alpha_l, \tau_l, \nu_l\}$ with L targets in a noiseless environment is $4L^2$, with $K \ge 2L$ and $P \ge 2L$.

Theorem 1 translates into requirements on the total bandwidth of the transmitted bands, such that

$$B_{\text{tot}} = N \sum_{i=1}^{N_b} \left\lceil \frac{B_r^i}{B_h} \right\rceil \ge 2L. \tag{42}$$

It is further shown in [36] that Doppler focusing increases the per-target SNR by P times. This linear scaling is similar to that obtained by using a matched filter. For the specific case of time delay estimation, Mishra and Eldar [63] compare the performance of conventional and CRrs using the extended Ziv-Zakai lower bound (EZB). In a conventional radar, the EZB for a single target delay estimate $\hat{\tau}_0$ is

$$\text{EZB}_R(\hat{\tau}_0) = \sigma_{\tau_0}^2 \cdot 2Q\left(\sqrt{\frac{\text{SNR}}{2}}\right) + \frac{\Gamma_{3/2}\left(\frac{\text{SNR}}{4}\right)}{\text{SNR} \cdot \overline{F}^2} \tag{43}$$

where $Q(\cdot)$ denotes the right-tail Gaussian probability function, $\Gamma_a(b)$ is the incomplete gamma function with parameter a and upper limit b, and $\overline{F}$ is the root-mean-square (rms) bandwidth of the full-band signal. The corresponding bound for a CRr is [63]

$$\text{EZB}_{\text{CRr}}(\hat{\tau}_0) = \sigma_{\tau_0}^2 \cdot 2Q\left(\sqrt{\frac{\widetilde{\text{SNR}}}{2}}\right) + \frac{\Gamma_{3/2}\left(\frac{\widetilde{\text{SNR}}}{4}\right)}{\sum_{i=1}^{N_b} \text{SNR}_i \cdot \overline{F_i^2}} \tag{44}$$

where SNR_i and $\overline{F_i}$ are the in-band SNR and rms bandwidth of the ith subband and $\widetilde{\text{SNR}}$ is the total SNR. As noted in [63], since $\sum_{i=1}^{N_b} B_r^i \subset B_h$, we have $\widetilde{\text{SNR}} > \text{SNR}$ for a given power P_T. Therefore, the SNR threshold for asymptotic performance of EZB_{CRr} is lower than EZB_R. As the noise increases and power remains constant for both radars, the asymptotic performance of EZB_{CRr} is more tolerant to the noise than EZB_R.

The multiband design strategy, besides allowing a dynamic form of the transmitted signal spectrum over only

Algorithm 4: Spectral Coexistence via Xampling (SpeCX).
Input: Comm signal $x_C(t)$
Output: Estimated target parameters $\{\hat{\alpha}_l, \hat{\tau}_l, \hat{v}_l\}_{l=0}^{L-1}$
1: Initialization: perform spectrum sensing at the receiver on $x_C(t)$ using Algorithm 1 with $S_R = \emptyset$
2: Choose the least noisy subbands for the radar transmit spectrum with respect to detected $\mathcal{F}_C$ using Algorithm 2
3: Communicate the transmitted radar signal support $\mathcal{F}_R$ to the comm and radar receivers
4: Perform target delay and Doppler estimation using Algorithm 3
5: Perform spectrum sensing at the comm receiver on $x(t) = x_C(t) + x_R(t)$ using Algorithm 1
6: If $\mathcal{F}_C$ changes, then the radar transmitter goes back to step 2

Fig. 5. Detection performance of the comm receiver in the presence of a radar signal with known support.

a small portion of the whole bandwidth to enable spectrum sharing, has two additional advantages. First, as we show in hardware experiments (see Section VI.B), our CS reconstruction achieves the same resolution as traditional Nyquist processing over a significantly smaller bandwidth. Second, since we only use narrow bands to transmit, the entire power is concentrated in them. Therefore, the SNR in the sampled bands is improved.

Our resulting spectrum sharing SpeCX framework is summarized in Algorithm 4.

VI. SOFTWARE AND HARDWARE EXPERIMENTS

In this section, we present software and hardware simulations to illustrate our SpeCX framework. Software experiments illustrate the comm band detection performance of the CRo and target detection by the CRr. Hardware simulations demonstrate a practical implementation of the SpeCX system.

A. Software Simulations

To test the radio receiver, we consider a comm signal composed of $N_{\text{sig}} = 2$ transmissions and a radar signal composed of $N_b = 4$ bands with known support. The Nyquist rate is $f_{\text{Nyq}} = 10$ GHz. Each comm transmission has a two-sided bandwidth $B_c^i = 50$ MHz and is modulated with a carrier f_c^i drawn uniformly at random between $\pm f_{\text{Nyq}}/2 = \pm 5$ GHz. The CRo receiver is composed of $M = 25$ analog channels, each sampling at rate $f_s = 154$ MHz and with $K = 91$ samples per channel. This leads to $N = 195$ spectral bands. Fig. 5 shows the performance of the detector for different values of the SNR, where the probability of detection is computed as the ratio of the correctly detected support. It can be seen that OMP-PKS, which exploits the knowledge of the radar signal's support, outperforms traditional OMP, as expected. The figures also present the performance of the comm receiver using OMP while the radar is silent. It can be seen that at low SNRs, the performance of OMP for both cases where the radar
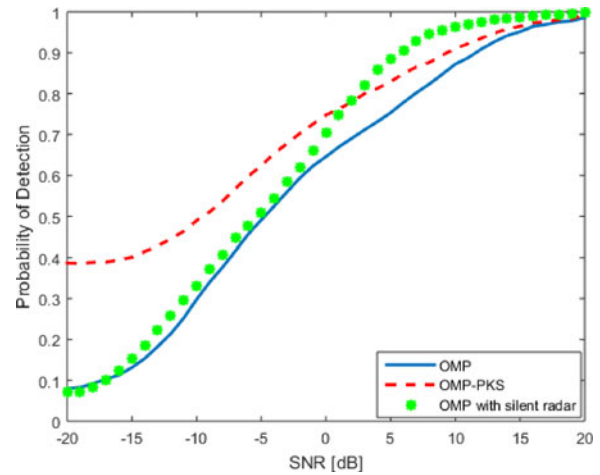
is present or absent is similar. In this regime, OMP-PKS outperforms both due to the additional knowledge about the radar support, whereas in the setting where the radar is silent, these bands are noisy, impairing OMP's performance. At high SNRs, the performance of OMP with a silent radar is the best. In this scenario, all bands that are not occupied by comm signals are close to empty. When the radar transmits, even though OMP-PKS has prior knowledge about the radar support, the signal itself is unknown as the received radar echoes from the targets are partially unknown (see step 6 Algorithm 1), so that the detection performance is a little lower than that of the silent radar case.

For the radar receiver, we consider a transmission with $N_b = 4$ spectral bands, each of bandwidth 81 kHz, yielding a total bandwidth of 324 kHz. We consider 4 combinations of transmit subbands with the frequency ranges, in kilohertz, of ([1–81], [8–162], [1663–1743], [1744–1824]), ([1–81], [582–662], [1663–1743], [1744–1824]), ([1–81], [82–162], [663–743], [1744–1824]), and ([1–81], [82–162], [163–243], [1744–1824]). For comparison, we simulate a wideband Nyquist pulse Doppler radar transmitting over a bandwidth $B_h = 1.62$ MHz. The CRr thus transmits over only 20% of the wideband. We consider $P = 100$ pulses with PRI $\tau = 10\,\mu$s. We use a hit-or-miss criterion as performance metric. A "hit" is defined as a delay-Doppler estimate circumscribed by an ellipse around the true target position in the time–frequency plane. We used ellipses with axes equivalent to ± 3 times the time and frequency Nyquist bins, defined as $1/B_h$ and $1/P\tau$, respectively. Fig. 6 shows the hit rate performance of our recovery method for the four different combinations of the transmitted spectral subbands, which outperforms traditional wideband radar transmission and processing. Obviously, transmitting over adjacent bands ([1–324] kHz) yields poor results.

B. Hardware Demo

The SpeCX prototype, shown in Fig. 7, is composed of a CRo receiver and a CRr transceiver. The CRo hardware
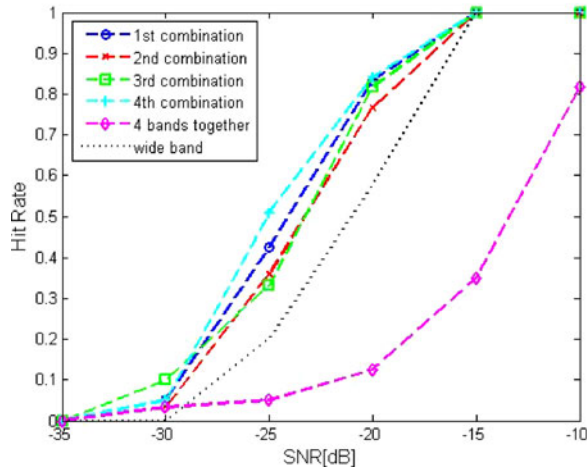
Fig. 6. Hit rate of multiband versus wideband radar. For the multiband configuration, the hit rate of four different combinations of transmit bands chosen at random, each with bandwidth 81 kHz, is shown, as well as that of four adjacent bands. The wideband radar transmits over a bandwidth of $B_h = 1.62$ MHz.
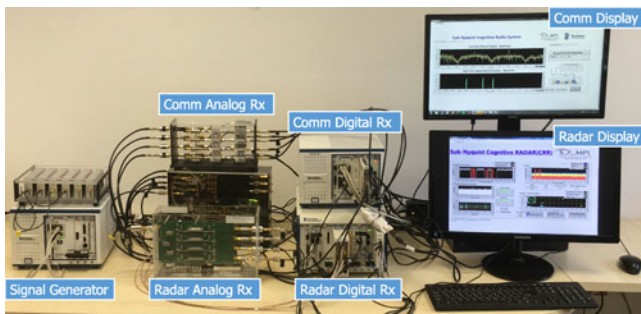

Fig. 7. Shared spectrum prototype. The system is composed of a signal generator, a CRo comm analog receiver including the MWC analog front-end board and the FPGA mixing sequences generator, a comm digital receiver, a CRr analog, and digital receiver.

realizes the system shown in Fig. 3. At the heart of the system lies our proprietary MWC board [65] that implements the sub-Nyquist analog front-end receiver. The card first splits the wideband signal into $M = 4$ hardware channels, with an expansion factor of $q = 5$, yielding $Mq = 20$ virtual channels after digital expansion. In each channel, the signal is then mixed with a periodic sequence $p_i(t)$, generated on a dedicated FPGA, with $f_p = 20$ MHz. The sequences are chosen as truncated versions of Gold Codes [82], commonly used in telecommunication (CDMA) and satellite navigation (GPS). These were heuristically found to give good detection results in the MWC system [83], primarily due to small bounded cross correlations within a set. This is useful when multiple devices are broadcasting in the same frequency range.

Next, the modulated signal passes through an analog antialiasing LPF. Specifically, a Chebyshev LPF of seventh order with a cutoff frequency (-3 dB) of 50 MHz was chosen for the implementation. Finally, the low rate analog signal is sampled by a National Instruments ADC operating at $f_s = (q + 1)f_p = 120$ MHz (with intended oversampling), leading to a total sampling rate of 480 MHz. The

digital receiver is implemented on a National Instruments PXIe-1065 computer with dc coupled ADC. Since the digital processing is performed at the low rate 120 MHz, very low computational load is required in order to achieve real-time recovery. MATLAB and LabVIEW platforms are used for the various digital recovery operations.

The prototype is fed with RF signals composed of up to $N_{\text{sig}} = 5$ real comm transmissions, namely $K = 10$ spectral bands with total bandwidth occupancy of up to 200 MHz and varying support, with Nyquist rate of 6 GHz. Specifically, to test the system's support recovery capabilities, an RF input is generated using vector signal generators, each producing a modulated data channel with individual bandwidth of up to 20 MHz and carrier frequencies ranging from 250 MHz up to 3.1 GHz. The input transmissions then go through an RF combiner, resulting in a dynamic multiband input signal, that enables fast carrier switching for each of the bands. This input is specially designed to allow testing the system's ability to rapidly sense the input spectrum and adapt to changes, as required by modern CRo and shared spectrum standards, e.g., in the SSPARC program. The system's effective sampling rate, equal to 480 MHz, is only 8% of the Nyquist rate and 2.4 times the Landau rate. This rate constitutes a relatively small oversampling factor of 20% with respect to the theoretical lower sampling bound. The main advantage of the Xampling framework, demonstrated here, is that sensing is performed in real time from sub-Nyquist samples for the entire spectral range, which results in substantial savings in both computational and memory complexity.

Support recovery is digitally performed on the low rate samples. The prototype successfully recovers the support of the comm transmitted bands, as demonstrated in Fig. 8. Once the support is recovered, the signal itself can be reconstructed from the sub-Nyquist samples in real time. We note that the reconstruction does not require interpolation to the Nyquist rate and the active transmissions are recovered at the low rate of 20 MHz, corresponding to the bandwidth of the slices $\mathbf{z}(f)$.

By combining both spectrum sensing and signal reconstruction, the MWC prototype serves as two separate comm devices. The first is a state-of-the-art CRo that performs real-time spectrum sensing at sub-Nyquist rates, and the second is a unique receiver able to decode multiple data transmissions simultaneously, regardless of their carrier frequencies, while adapting to spectral changes in real time.

The CRr system [36]–[38] includes a custom made sub-Nyquist radar receiver board composed of $N_b = 4$ parallel channels that sample $N_b = 4$ distinct bands of the radar signal spectral content. In the ith channel, the transmitted band with center frequency f_r^i and bandwidth $B_r^i = 80$ kHz is filtered, demodulated to baseband, and sampled at 250 kHz (with intentional oversampling). This way, four sets of consecutive Fourier coefficients are acquired. More details on the hardware design can be found in [38]. After sampling, the spectrum of each channel output is computed via FFT and the 320 Fourier coefficients are used for digital recovery of the delay-Doppler map [36]. The prototype simulates
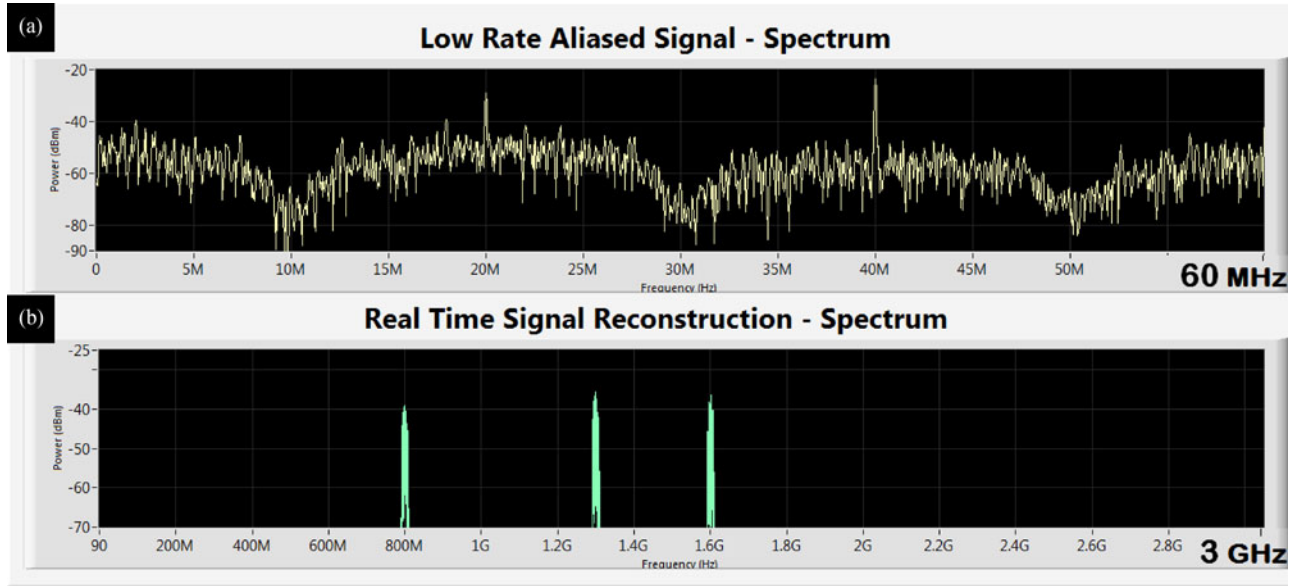
Fig. 8. SpeCX comm system display showing (a) low rate samples acquired from one MWC channel at rate 120 MHz and (b) digital reconstruction of the entire spectrum from sub-Nyquist samples.

transmission of $P = 50$ pulses towards $L = 9$ targets. The CRr transmits over $N_b = 4$ bands, selected according to the procedure presented in Section V-A, after the spectrum sensing process has been completed by the comm receiver. We compare the target detection performance of our CRr with a traditional wideband radar with bandwidth $B_h = 20\,\text{MHz}$. The CRr transmitted bandwidth is thus equal to 3.2% of the wideband.

Fig. 9 shows windows from the GUI of our CRr system. Fig. 9(a) illustrates the coexistence between the radar transmitted bands in red and the existing comm bands in white. The gain in power is demonstrated in Fig. 9(b); the wideband radar spectrum is shown in blue, our CRr in red, and the noise in yellow in a logarithmic scale. The true and recovered range-Doppler maps for the CRr whose transmit signal consists of four disjoint subbands are shown in Fig. 9(c). All nine targets are perfectly recovered and clutter, shown in yellow, is discarded. Fig. 9(d) shows the performance when the four subbands are joined together to result in a 320-kHz contiguous band for the radar transmitter. There are many missed detections and false alarms in this case.

Let the true and estimated ranges of the ith target be d_i and $\hat{d}_i$, respectively. Then, the root-mean-square localization error (RMSLE) of L targets is given by

$$\text{RMSLE} = \sqrt{\frac{1}{L} \sum_{i=1}^{L} (d_i - \hat{d}_i)^2}. \quad (45)$$

In Fig. 9(c) and (d), the RMSLE is shown as follows: CRr (0.34 km), 320-kHz band or four adjacent bands with same bandwidth (8.1km), and wideband (1.2km). The poor resolution of the four adjacent bands scenario is due to its small aperture. The native range resolution in case of 2-MHz wideband scenario is 75 m. In Fig. 9(c), the CRr is able
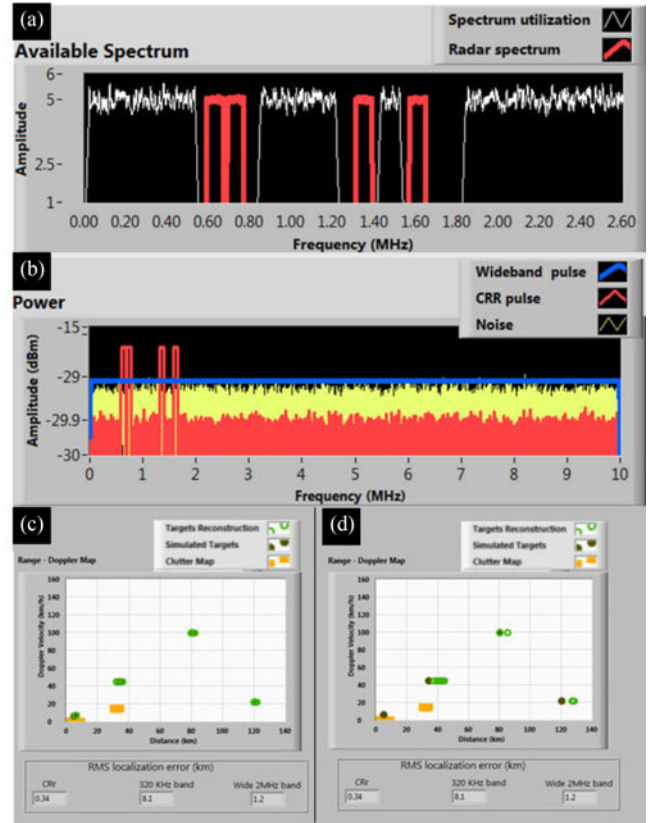

Fig. 9. SpeCX radar display showing (a) coexisting comm and CRr and (b) CRr spectrum compared with the full-band radar spectrum. The range-Doppler display of detected and true locations of the targets for the case of (c) CRr (four disjoint bands) and (d) all four transmit subbands together forming a contiguous 320-kHz band.

to detect nine targets at locations 6.097, 31.764, 35.046, 35.451, 35.479, 81.049, 81.570, 121.442, and 120.922 km. Here, the distance between two closely spaced targets is

less than 75 m. This empirically shows that our CRr system with nonadjacent bands yields better resolution than the traditional wideband scenario.

VII. SUMMARY

Our SpeCX model proposes a comm and radar spectral coexistence approach through the well-established theory of Xampling. We demonstrated that the two networks can actively cooperate through handshaking of information on the RF environment and optimize their performances. Unlike previous approaches, we presented a complete solution that shows signal recovery in both systems with minimal known information about the spectrum. We showed that the SpeCX is practically feasible through the development and real-time testing of our hardware prototype.

Some elements of the signal model that were not considered in this paper include performance of the comm receiver when the radar signal is also contaminated with clutter and hostile jamming. Extensions to MIMO radar–comm spectrum sharing as described by [14] are also interesting. Here, we may utilize the cognitive sub-Nyquist MIMO radar developed in [84]. It would also be useful to incorporate additional optimization constraints into the radar waveform design.

REFERENCES

[1] H. Griffiths *et al.*
Radar spectrum engineering and management: Technical and regulatory issues
in Proc. IEEE, vol. 103, no. 1, pp. 85–102, Jan. 2015.

[2] M. P. Fitz, T. R. Halford, I. Hossain, and S. W. Enserink
Towards simultaneous radar and spectral sensing
In *Proc. IEEE Int. Symp. Dyn. Spectr. Access Netw.*, 2014, pp. 15–19.

[3] J. Bernhard, J. Reed, J. M. Park, A. Clegg, A. Weisshaar, and A. Abouzeid
Final report of the National Science Foundation workshop on Enhancing Access to the Radio Spectrum (EARS)
Nat. Sci. Found., Arlington, VA, USA, Tech. Rep., 2010.

[4] G. M. Jacyna, B. Fell, and D. McLemore
A high-level overview of fundamental limits studies for the DARPA SSPARC program
In *Proc. IEEE Radar Conf.*, 2016, pp. 1–6.

[5] J. R. Guerci, R. M. Guerci, A. Lackpour, and D. Moskowitz
Joint design and operation of shared spectrum access for radar and communications
In *Proc. IEEE Radar Conf.*, 2015, pp. 0761–0766.

[6] S. C. Surender, R. M. Narayanan, and C. R. Das
Performance analysis of communications & radar coexistence in a covert UWB OSA system
In *Proc. IEEE Global Telecommun. Conf.*, 2010, pp. 1–5.

[7] L. K. Patton, C. A. Bryant, and B. Himed
Radar-centric design of waveforms with disjoint spectral support
In *Proc. IEEE Radar Conf.*, 2012, pp. 269–274.

[8] P. Stinco, M. S. Greco, and F. Gini
Spectrum sensing and sharing for cognitive radars
IET Radar, Sonar Navig., vol. 10, no. 3, pp. 595–602, 2016.

[9] N. Nartasilpa, D. Tuninetti, N. Devroye, and D. Erricolo
Let's share CommRad: Effect of radar interference on an uncoded data communication system
In *Proc. IEEE Radar Conf.*, 2016, pp. 1–5.

[10] J. G. Metcalf, C. Sahin, S. D. Blunt, and M. Rangaswamy
Analysis of symbol-design strategies for intrapulse radar-embedded communications
IEEE Trans. Aerosp. Electron. Syst., vol. 51, no. 4, pp. 2914–2931, Oct. 2015.

[11] A. R. Chiriyath, B. Paul, G. M. Jacyna, and D. W. Bliss
Inner bounds on performance of radar and communications co-existence
IEEE Trans. Signal Process., vol. 64, no. 2, pp. 464–474, Jan. 2015.

[12] J. T. Reed, J. L. Odom, R. T. Causey, and A. D. Lanterman
Gaussian multiple access channels for radar and communications spectrum sharing
In *Proc. IEEE Radar Conf.*, 2016, pp. 1–6.

[13] C. D. Richmond, P. Basu, R. E. Learned, J. Vian, A. Worthen, and M. Lockard
Performance bounds on cooperative radar and communication systems operation
In *Proc. IEEE Radar Conf.*, 2016, pp. 1–6.

[14] B. Li, A. P. Petropulu, and W. Trappe
Optimum co-design for spectrum sharing between matrix completion based MIMO radars and a MIMO communication system
IEEE Trans. Signal Process., vol. 64, no. 17, pp. 4562–4575, Sep. 2016.

[15] C. Sturm and W. Wiesbeck
Waveform design and signal processing aspects for fusion of wireless communications and radar sensing
in Proc. IEEE, vol. 99, no. 7, pp. 1236–1259, Jul. 2011.

[16] P. Kumari, N. González-Prelcic, and R. W. Heath
Investigating the IEEE 802.11ad standard for millimeter wave automotive radar
In *Proc. IEEE Veh. Technol. Conf.*, 2015, pp. 1–5.

[17] M. Davis
Foliage Penetration Radar: Detection and Characterization of Objects Under Trees. London, U.K.: Inst. Eng. Technol., 2011.

[18] K. Gerlach
Thinned spectrum ultrawideband waveforms using stepped-frequency polyphase codes
IEEE Trans. Aerosp. Electron. Syst., vol. 34, no. 4, pp. 1356–1361, Oct. 1998.

[19] H. He, J. Li, and P. Stoica
Waveform Design for Active Sensing Systems: A Computational Approach. Cambridge, U.K.: Cambridge Univ. Press, 2012.

[20] C. Nunn and L. R. Moyer
Spectrally-compliant waveforms for wideband radar
IEEE Aerosp. Electron. Syst. Mag., vol. 27, no. 8, pp. 11–15, Aug. 2012.

[21] W. Rowe, P. Stoica, and J. Li
Spectrally constrained waveform design
IEEE Signal Process. Mag., vol. 31, no. 3, pp. 157–162, May 2014.

[22] A. Aubry, A. De Maio, M. Piezzo, and A. Farina
Radar waveform design in a spectrally crowded environment via nonconvex quadratic optimization
IEEE Trans. Aerosp. Electron. Syst., vol. 50, no. 2, pp. 1138–1152, Apr. 2014.

[23] G. Wang and Y. Lu
Designing single/multiple sparse frequency waveforms with sidelobe constraint
IET Radar, Sonar, Navig., vol. 5, no. 1, pp. 32–38, Jan. 2011.

[24] M. J. Lindenfeld
Sparse frequency transmit-and-receive waveform design
IEEE Trans. Aerosp. Electron. Syst., vol. 40, no. 3, pp. 851–861, Jul. 2004.

[25] H. He, P. Stoica, and J. Li
Waveform design with stopband and correlation constraints for cognitive radar
In *Proc. Int. Workshop Cogn. Inf. Process.*, 2010, pp. 344–349.

[26] K.-W. Huang, M. Bică, U. Mitra, and V. Koivunen
Radar waveform design in spectrum sharing environment: Co-existence and cognition
In *Proc. IEEE Radar Conf.*, 2015, pp. 1698–1703.

[27] P. S. Tan, J. M. Stiles, and S. D. Blunt
Optimizing sparse allocation for radar spectrum sharing
In *Proc. IEEE Radar Conf.*, 2016, pp. 1–6.

[28] A. Aubry, A. De Maio, Y. Huang, M. Piezzo, and A. Farina
A new radar waveform design algorithm with improved feasibility for spectral coexistence
IEEE Trans. Aerosp. Electron. Syst., vol. 51, no. 2, pp. 1029–1038, Apr. 2015.

[29] M. Mishali, Y. C. Eldar, and A. J. Elron
Xampling: Signal acquisition and processing in union of subspaces
IEEE Trans. Signal Process., vol. 59, no. 10, pp. 4719–4734, Oct. 2011.

[30] Y. C. Eldar
Sampling Theory: Beyond Bandlimited Systems. Cambridge, U.K.: Cambridge Univ. Press, 2015.

[31] Y. C. Eldar and G. Kutyniok
Compressed Sensing: Theory and Applications. Cambridge, U.K.: Cambridge Univ. Press, 2012.

[32] M. Mishali and Y. C. Eldar
From theory to practice: Sub-Nyquist sampling of sparse wideband analog signals
IEEE J. Sel. Topics Signal Process., vol. 4, no. 2, pp. 375–391, Apr. 2010.

[33] M. Mishali and Y. C. Eldar
Sub-Nyquist sampling
IEEE Signal Process. Mag., vol. 28, no. 6, pp. 98–124, Nov. 2011.

[34] D. Cohen and Y. C. Eldar
Sub-Nyquist sampling for power spectrum sensing in cognitive radios: A unified approach
IEEE Trans. Signal Process., vol. 62, no. 15, pp. 3897–3910, Aug. 2014.

[35] D. Cohen and Y. C. Eldar
Sub-Nyquist cyclostationary detection for cognitive radio
IEEE Trans. Signal Process., vol. 65, no. 11, pp. 3004–3019, Jun. 2017.

[36] O. Bar-Ilan and Y. C. Eldar
Sub-Nyquist radar via Doppler focusing
IEEE Trans. Signal Process., vol. 62, no. 7, pp. 1796–1811, Apr. 2014.

[37] D. Cohen, A. Dikopoltsev, R. Ifraimov, and Y. C. Eldar
Towards sub-Nyquist cognitive radar
In *Proc. IEEE Radar Conf.*, 2016, pp. 1–4.

[38] E. Baransky, G. Itzhak, I. Shmuel, N. Wagner, E. Shoshan, and Y. C. Eldar
A sub-Nyquist radar prototype: Hardware and applications
IEEE Trans. Aerosp. Electron. Syst., vol. 50, no. 2, pp. 809–822, Apr. 2014.

[39] J. Mitola and C. Q. Maguire, Jr.
Cognitive radio: Making software radios more personal
IEEE Pers. Commun., vol. 6, no. 4, pp. 13–18, Aug. 1999.

[40] S. Haykin
Cognitive radio: Brain-empowered wireless communications
IEEE J. Sel. Areas Commun., vol. 23, no. 2, pp. 201–220, Feb. 2005.

[41] E. Axell, G. Leus, E. G. Larsson, and H. V. Poor
Spectrum sensing for cognitive radios: State-of-the-art and recent advances
IEEE Signal Process. Mag., vol. 29, no. 3, pp. 101–116, May 2012.

[42] S. K. Sharma, E. Lagunas, S. Chatzinotas, and B. Ottersten
Application of compressive sensing in cognitive radio communications: A survey
IEEE Commun. Surveys Tuts., vol. 18, no. 3, pp. 1838–1860, Jul.–Sep. 2016.

[43] D. Cohen, S. Tsiper, and Y. C. Eldar
Analog to digital cognitive radio
In *Handbook of Cognitive Radio*, W. Zhang, Ed. Singapore: Springer, 2017.

[44] D. Cohen, S. Tsiper, and Y. C. Eldar
Analog to digital cognitive radio: Sampling, detection and hardware
IEEE Signal Process. Mag., vol. 35, no. 1, pp. 137–166, Jan. 2018.

[45] J. D. Taylor
Ultra-wideband Radar Technology. Boca Raton, FL, USA: CRC Press, 2000.

[46] Z. Khan, J. J. Lehtomaki, R. Vuohtoniemi, E. Hossain, and L. A. Dasilva
On opportunistic spectrum access in radar bands: Lessons learned from measurement of weather radar signals
IEEE Wireless Commun., vol. 23, no. 3, pp. 40–48, Jun. 2016.

[47] P. Stinco, M. S. Greco, and F. Gini
White space passive coherent location system based on IEEE 802.22
In *Proc. IEEE Int. Radar Symp.*, 2015, pp. 71–76.

[48] P. Stinco, M. S. Greco, F. Gini, and B. Himed
IEEE 802.22 passive radars: Multistatic detection and velocity profiler
IEEE Trans. Aerosp. Electron. Syst., vol. 52, no. 5, pp. 2298–2313, Oct. 2016.

[49] P. Stinco, M. S. Greco, F. Gini, and B. Himed
ComRadE: Cognitive passive tracking in symbiotic IEEE 802.22 systems
IEEE Trans. Aerosp. Electron. Syst., vol. 53, no. 2, pp. 1023–1034, Apr. 2017.

[50] H. Wang, J. Johnson, C. Baker, L. Ye, and C. Zhang
On spectrum sharing between communications and air traffic control radar systems
In *Proc. IEEE Radar Conf.*, 2015, pp. 1545–1550.

[51] M. La Manna, P. Stinco, M. Greco, and F. Gini
Design of a cognitive radar for operation in spectrally dense environments
In *Proc. IEEE Radar Conf.*, 2013, pp. 1–6.

[52] F. Hessar and S. Roy
Spectrum sharing between a surveillance radar and secondary Wi-Fi networks
IEEE Trans. Aerosp. Electron. Syst., vol. 52, no. 3, pp. 1434–1448, Jun. 2016.

[53] J. H. Reed *et al.*
On the co-existence of TD-LTE and radar over 3.5 GHz band: An experimental study
IEEE Wireless Commun. Lett., vol. 5, no. 4, pp. 368–371, Aug. 2016.

[54] M. Labib, J. H. Reed, A. F. Martone, and A. I. Zaghloul
Coexistence between radar and LTE-U systems: Survey on the 5 GHz band
In *Proc. United States Nat. Committee URSI Nat. Radio Sci. Meeting*, 2016, pp. 1–2.

[55] E. Saltikoff *et al.*
The threat to weather radars by wireless technology
Bull. Amer. Meteorol. Soc., vol. 97, no. 7, pp. 1159–1167, 2016.

[56] Y. Han, E. Ekici, H. Kremo, and O. Altintas
Optimal spectrum utilization in joint automotive radar and communication networks
In *Proc. Int. Symp. Model. Optim. Mobile Ad Hoc Wireless Netw.*, 2016, pp. 1–8.

[57] M. Heddebaut *et al.*
Millimeter-wave communicating-radars for enhanced vehicle-to-vehicle communications
Transp. Res., C, Emerg. Technol., vol. 18, no. 3, pp. 440–456, 2010.

[58] J. Mitola *et al.*
Accelerating 5G QoE via public-private spectrum sharing

IEEE Commun. Mag., vol. 52, no. 5, pp. 77–85, May 2014.

[59] K. V. Mishra, A. Zhitnikov, and Y. C. Eldar
Spectrum sharing solution for automotive radar
In Proc. IEEE Veh. Technol. Conf., Spring, Jun. 2017.

[60] K. V. Mishra and Y. C. Eldar
Sub-Nyquist channel estimation over IEEE 802.11ad link
In Proc. IEEE Int. Conf. Sampling Theory Appl., 2017, pp. 355–359.

[61] M. Mishali and Y. C. Eldar
Blind multi-band signal reconstruction: Compressed sensing for analog signals
IEEE Trans. Signal Process., vol. 57, no. 3, pp. 993–1009, 2009.

[62] M. Skolnik
Radar Handbook. New York, NY, USA: McGraw-Hill, 1970.

[63] K. V. Mishra and Y. C. Eldar
Performance of time delay estimation in a cognitive radar
In Proc. IEEE Int. Conf. Acoust., Speech Signal Process., 2017, pp. 3141–3145.

[64] H. Landau
Necessary density conditions for sampling and interpolation of certain entire functions
Acta Math., vol. 117, pp. 37–52, 1967.

[65] M. Mishali, Y. C. Eldar, O. Dounaevsky, and E. Shoshan
Xampling: Analog to digital at sub-Nyquist rates
IET Circuits, Devices Syst., vol. 5, pp. 8–20, 2011.

[66] N. Vaswani and W. Lu
Modified-CS: Modifying compressive sensing for problems with partially known support
IEEE Trans. Signal Process., vol. 58, no. 9, pp. 4595–4607, Sep. 2010.

[67] N. Vaswani and J. Zhan
Recursive recovery of sparse signal sequences from compressive measurements: A review
IEEE Trans. Signal Process., vol. 64, no. 13, pp. 3523–3549, Jul. 2016.

[68] V. Stankovi, L. Stankovi, and S. Cheng
Compressive image sampling with side information
In Proc. IEEE Int. Conf. Image Process., 2009, pp. 3037–3040.

[69] R. E. Carrillo, L. F. Polania, and K. E. Barner
Iterative algorithms for compressed sensing with partially known support
In Proc. IEEE Int. Conf. Acoust., Speech Signal Process., 2010, pp. 3654–3657.

[70] W. Lu and N. Vaswani
Regularized modified BPDN for noisy sparse reconstruction with partial erroneous support and signal value knowledge
IEEE Trans. Signal Process., vol. 60, no. 1, pp. 182–196, Jan. 2012.

[71] J. Fang, Y. Shen, F. Li, H. Li, and Z. Chen
Support knowledge-aided sparse Bayesian learning for compressed sensing
In Proc. IEEE Int. Conf. Acoust., Speech Signal Process., 2015, pp. 3786–3790.

[72] M. Shekaramiz, T. K. Moon, and J. H. Gunther
Sparse Bayesian learning boosted by partial erroneous support knowledge
In Proc. IEEE Asilomar Conf. Signals, Syst. Comput., 2016, pp. 389–393.

[73] S. M. Kay
Fundamentals of Statistical Signal Processing, Volume 2: Detection Theory. Englewood Cliffs, NJ, USA: Prentice Hall, 1998.

[74] J. Huang, T. Zhang, and D. Metaxas
Learning with structured sparsity
J. Mach. Learn. Res., vol. 12, no. Nov, pp. 3371–3412, 2011.

[75] L. Yu, H. Sun, J. P. Barbot, and G. Zheng
Bayesian compressive sensing for cluster structured sparse signals
Signal Process., vol. 92, no. 1, pp. 259–269, 2012.

[76] T. Peleg, Y. C. Eldar, and M. Elad
Exploiting statistical dependencies in sparse representations for signal recovery
IEEE Trans. Signal Process., vol. 60, no. 5, pp. 2286–2303, May 2012.

[77] J. Huang, X. Huang, and D. Metaxas
Learning with dynamic group sparsity
In Proc. IEEE Int. Conf. Comput. Vis., 2009, pp. 64–71.

[78] Z. Zhang and B. D. Rao
Sparse signal recovery with temporally correlated source vectors using sparse Bayesian learning
IEEE J. Sel. Topics Signal Process., vol. 5, no. 5, pp. 912–926, Sep. 2011.

[79] Z. Zhang and B. D. Rao
Recovery of block sparse signals using the framework of block sparse Bayesian learning
In Proc. IEEE Int. Conf. Acoust., Speech Signal Process., 2012, pp. 3345–3348.

[80] J. Fang, Y. Shen, H. Li, and P. Wang
Pattern-coupled sparse Bayesian learning for recovery of block-sparse signals
IEEE Trans. Signal Process., vol. 63, no. 2, pp. 360–372, Jan. 2015.

[81] L. L. Scharf and B. Friedlander
Matched subspace detectors
IEEE Trans. Signal Process., vol. 42, no. 8, pp. 2146–2157, Aug. 1994.

[82] R. Gold
Optimal binary sequences for spread spectrum multiplexing (Corresp.)
IEEE Trans. Inf. Theory, vol. 13, no. 4, pp. 619–621, Oct. 1967.

[83] M. Mishali and Y. C. Eldar
Expected RIP: Conditioning of the modulated wideband converter
In Proc. IEEE Inf. Theory Workshop, Oct. 2009, pp. 343–347.

[84] K. V. Mishra et al.
Cognitive sub-Nyquist hardware prototype of a collocated MIMO radar
In Proc. Int. Workshop Compressed Sens. Theory Appl. Radar, Sonar Remote Sens., 2016, pp. 56–60.

Deborah Cohen (S'13) received the B.Sc. degree (*summa cum laude*) in electrical engineering and the Ph.D. degree in electrical engineering from the Technion–Israel Institute of Technology, Haifa, Israel, in 2010 and 2016, respectively.

Since 2010, she has been a Project Supervisor with the Signal and Image Processing Laboratory, the High Speed Digital Systems Laboratory, the Communications Laboratory, and the Signal Acquisition, Modeling and Processing Lab, Electrical Engineering Department, Technion—Israel Institute of Technology. She is currently a Research Scientist with Google Research Israel, Tel Aviv, Israel. Her research interests include theoretical aspects of signal processing, compressed sensing, reinforcement learning, and machine learning for dialogues.

Dr. Cohen has been an Azrieli Fellow since 2014. She was the recipient of the Meyer Foundation Excellence prize, in 2011, the Sandor Szego Award and the Vivian Konigsberg Award for Excellence in Teaching from 2012 to 2016, the David and Tova Freud and Ruth Freud-Brendel Memorial Scholarship in 2014, and the Muriel and David Jacknow Award for Excellence in Teaching in 2015.

Kumar Vijay Mishra received the B. Tech. (Hons., Gold Medal) degree (*summa cum laude*) in electronics and communication engineering from the National Institute of Technology, Hamirpur, Hamirpur, India, in 2003, the Ph.D. in electrical engineering from University of Iowa, Iowa City, IA, USA, in 2015, the M.S. in electrical engineering from Colorado State University, Fort Collins, CO, USA, in 2012, while working on the NASA GPM-GV mission weather radars, and the M.S. degree in mathematics from The University of Iowa, Iowa City, IA, USA, in 2015.

He is currently an Andrew and Erna Finci Viterbi and Lady Davis Postdoctoral Fellow with the Faculty of Electrical Engineering, Technion–Israel Institute of Technology, Haifa, Israel. During 2003–2007, he was a Research Scientist with Electronics and Radar Development Establishment (LRDE), Bengaluru, India, in the air surveillance radars. In 2015, he was a Research Intern with Mitsubishi Electric Research Laboratories, Cambridge, MA, USA, and Qualcomm, San Jose, CA, USA. His research interests include radar systems theory and hardware, signal processing, radar polarimetry, remote sensing, and electromagnetics.

Dr. Mishra was the recipient of the Royal Meteorological Society Quarterly Journal Editor's Prize (2017), the Lady Davis Fellowship (2016–17), the Andrew and Erna Finci Viterbi Fellowship (twice awarded, in 2015 and 2016), the Technion Faculty of Electrical Engineering Excellent Undergraduate Mentor Award (2017), the Cornell Base-of-Pyramid Narrative Competition (2009), the LRDE Scientist of the Year Award (2006), and the NITH Best Student Award (2003).

Yonina C. Eldar (S'98–M'02–SM'07–F'12) received the B.Sc. degree in physics and the B.Sc. degree in electrical engineering, both from Tel Aviv University, Tel Aviv, Israel, and the Ph.D. degree in electrical engineering and computer science from the Massachusetts Institute of Technology (MIT), Cambridge, MA, USA, in 1995, 1996, and 2002, respectively.

She is currently a Professor with the Department of Electrical Engineering, Technion–Israel Institute of Technology, Haifa, Israel, where she holds the Edwards Chair in Engineering. She is also a Research Affiliate with the Research Laboratory of Electronics, MIT, an Adjunct Professor with Duke University, Durham, NC, USA, and was a Visiting Professor with Stanford University, Stanford, CA, USA. She is the author of the book *Sampling Theory: Beyond Bandlimited Systems* (Cambridge Univ. Press, 2015) and the coauthor of the books *Compressed Sensing* (Cambridge Univ. Press, 2012), and *Convex Optimization Methods in Signal Processing and Communications* (Cambridge Univ. Press, 2010). Her research interests include statistical signal processing, sampling theory and compressed sensing, optimization methods, and their applications to biology and optics.

Dr. Eldar is currently a Member of the Israel Academy of Sciences and Humanities (elected 2017) and a EURASIP Fellow. She was a Member of the Young Israel Academy of Science and Humanities and the Israel Committee for Higher Education. She was a Horev Fellow of the Leaders in Science and Technology program at the Technion and an Alon Fellow. She is currently the Editor-in-Chief for *Foundations and Trends in Signal Processing*, a Member of the IEEE Sensor Array and Multichannel Technical Committee, and serves on several other IEEE committees. In the past, she was a Signal Processing Society Distinguished Lecturer, a Member of the IEEE Signal Processing Theory and Methods and Bio Imaging Signal Processing technical committees, and served as an Associate Editor for the IEEE TRANSACTIONS ON SIGNAL PROCESSING, the *EURASIP Journal of Signal Processing*, the *SIAM Journal on Matrix Analysis and Applications*, and the *SIAM Journal on Imaging Sciences*. She was the Cochair and Technical Cochair of several international conferences and workshops. She was the recipient of many awards for excellence in research and teaching, including the IEEE Signal Processing Society Technical Achievement Award (2013), the IEEE/AESS Fred Nathanson Memorial Radar Award (2014), the IEEE Kiyo Tomiyasu Award (2016), the Michael Bruno Memorial Award from the Rothschild Foundation, the Weizmann Prize for Exact Sciences, the Wolf Foundation Krill Prize for Excellence in Scientific Research, the Henry Taub Prize for Excellence in Research (twice), the Hershel Rich Innovation Award (three times), the Award for Women with Distinguished Contributions, the Andre and Bella Meyer Lectureship, the Career Development Chair at the Technion, the Muriel & David Jacknow Award for Excellence in Teaching, and the Technions Award for Excellence in Teaching (twice). She was also the recipient of several best paper awards and best demo awards together with her research students and colleagues including the SIAM outstanding Paper Prize, the UFFC Outstanding Paper Award, the Signal Processing Society Best Paper Award, and the IET Circuits, Devices and Systems Premium Award. She was selected as one of the 50 most influential women in Israel.